Physica Scripta

PAPER

# Optical properties of donor impurity in Yukawa like potential: application to *SiGe/Si* and *Si/SiGe*

**Varsha**[1,2,*], **M Kria**[3], **Vijit V Nautiyal**[1], **K Lakaal**[3], **D Laroze**[4], **L M Pérez**[5], **V Prasad**[6,*] and **E Feddi**[3,7,*]

[1] Department of Physics and Astrophysics, University of Delhi, Delhi—110007, India
[2] Department of Physics, Kalindi College, University of Delhi, Delhi—110008, India
[3] Group of Optoelectronic of Semiconductors and Nanomaterials, ENSAM, Mohammed V University in Rabat, Morocco
[4] Instituto de Alta Investigación, CEDENNA, Universidad de Tarapacá, Casilla 7 D, Arica, Chile
[5] Departamento de Física, FACI, Universidad de Tarapacá, Casilla 7 D, Arica, Chile
[6] Department of Physics, Swami Shraddhanand College, University of Delhi, Delhi—110036, India
[7] Institute of Applied Physics, Mohammed VI Polytechnic University, Lot 660, Hay Moulay Rachid Ben Guerir, 43150, Morocco
[*] Authors to whom any correspondence should be addressed.

**E-mail:** varsha.yadav610@gmail.com, vprasad@ss.du.ac.in and e.feddi@um5r.ac.ma

**Keywords:** quantum dot, refractive index changes, absorption coefficient

**RECEIVED**
17 November 2022

**REVISED**
17 March 2023

**ACCEPTED FOR PUBLICATION**
27 March 2023

**PUBLISHED**
6 April 2023

## Abstract

We have investigated the effect of temperature and geometrical confinement on the behavior of spherical cavities with Yukawa potential presence inside the cavity within effective mass approximation. Using the Finite-element method, we have calculated the energy eigenvalue with the geometric and temperature effects into consideration with consideration of temperature and position-dependent mass, and position-dependent dielectric constant. The optical transition from the ground to the excited state shows a blueshift in optical absorption coefficient, refractive index changes, and second and third harmonic generation with an increase in temperature. The increase in the geometric size of the spherical cavity causes a redshift in the optical resonance peaks.

## 1. Introduction

The study of quantum heterostructures has had a special place in research since its discovery due to its relevance in different technologies and fields [1–10]. Quantum heterostructures' response to external fields is an area of increasing interest as these external fields include pressure, temperature, electric fields, magnetic fields, laser fields, etc [11–15] are the tools to manipulate the optoelectronic properties and amend them to our advantage. We can exploit these electronic and optical properties as per the requirements of the optoelectronic device by tuning these parameters. Another way is to make changes in the shape and size of the heterostructure [16–23] but these fabrication techniques are expensive and time-consuming so these external fields come in handy. In the literature, several studies are devoted to this field, a few of which are given in references [24–27]. In 1998, Perlin *et al* [28] used probes like pressure, temperature, and excitation power to study InGaN/GaN quantum wells. Their study reported a characteristic 'blueshift' with increasing pumping power in the energies of photo- and electro-luminescence transitions in InGaN quantum wells which have been attributed either to band-tail filling or to a screening of piezoelectric fields. P. Dawson *et al* [29] studied temperature-dependent optical properties of InAs/GaAs quantum dots both theoretically and experimentally. The authors reported that carrier dynamics are governed by independent carrier relaxation at elevated temperatures. The optical properties of a hydrogenic impurity in a disc-shaped quantum dot with effects of hydrostatic pressure and temperature with parabolic confinement in the presence of an external electric field were studied by Liang and Xie [30]. The authors showed that with increasing pressure both the total absorption coefficient and the refractive index change cause a blueshift and redshift for donor and acceptor impurities respectively. However, the reverse is observed with increasing temperature. Kirak *et al* [31] studied the non-linear optical properties in the presence of the electric field, hydrostatic pressure, and temperature for a spherical QD with parabolic confinement using

© 2023 IOP Publishing Ltd

the variational method in the frame of the effective mass approximation. Redshift is observed for increasing pressure at a constant temperature and blueshift is observed when the temperature is increased at a constant pressure.

The Yukawa potential is useful as it can be used for describing strong interactions between nucleons, in plasma physics for describing the potential of a charged particle in a weakly non-ideal plasma, in electrolytes and colloids, in solid state physics for describing the effects of a charged particle in a sea of conduction electrons and as well as in quantum mechanics [32]. To show the applicability of this potential, a few of the studies are mentioned here. Lumb *et al* [33] studied photoexcitation and ionization of a hydrogen atom confined by a combined effect of a spherical box and Debye plasma by solving the Schrödinger equation by using Bernstein-polynomials (B-polynomials). They reported that the confining spherical box and the screening parameter of Debye plasma affect photoexcitation and ionization. In reference [34], the authors in the presence of static magnetic and electric fields studied the bound state energy of spherical quantum dots with Yukawa potential using the Ansatz Methods approach and gave analytical expressions for the energy levels and radial wavefunction of the system. Camacho *et al* [35] studied GaAs quantum wires with two electrons in a conduction band whose interaction is modeled using the Yukawa potential. They verified experimental results available for Wigner crystal formation in InSb and InAs nanowires using their model. In nanophotonics, optical near-field interactions allow electric-dipole forbidden transitions. The matter interaction in such systems has been successfully studied experimentally using Yukawa's potential [36, 37]. This implies that Yukawa's potential is effective for modeling systems in real-time scenario systems. The studies in references [38–42] show the diversity of this potential and its application. Therefore, in the present manuscript, we have studied the optical properties of a donor impurity in Yukawa like the potential for *SiGe/Si* (*Si/SiGe*) QD. In the next section, we gave the detailed theory required for the understanding of the system followed by the results obtained with discussion. In the end, we concluded our work by giving its importance.

## 2. Theory

$Si_{1-x}Ge_x$ QD within *Si* matrix and vice-versa with an ionized donor impurity at the center is considered for the study where $x = 0.3$ as shown in figure 1.

The effective mass of electron for Si, along longitudinal ($m_l$) is $0.92m_0$ and along transverse ($m_t$) is equal to $0.19m_0$ and for Ge, $m_l = 1.64m_0$ and $m_t = 0.082m_0$. The dielectric strength as a composition of $x$ is given by $\epsilon(x) = 11.9(1 + 0.35\,x)$ [27, 43, 44].

The eigen-energies and corresponding wave functions are solutions of the Schrödinger equation:

$$\frac{-\hbar^2}{2}\nabla\left[\frac{1}{m_i^*(r)}\nabla\psi(r)\right] + V_w^e(r)\psi(r) + V_c(r)\psi(r) = E\psi(r) \tag{1}$$

where the wave functions and the energy levels, respectively, are $\psi(r)$ and $E$. The position-dependent effective mass of the electron, $m_i^*$, which is different for the matrix and QD area, is given by [44]:

$$m_i^* = \begin{cases} m_{SiGe}^* & \text{inside the core and the WL} \\ m_{Si}^* & \text{otherwise} \end{cases} \tag{2}$$

Similar to this, the coulombic potential $V_c(r)$ and the confining potential, $V_w^e(r)$ energy is given by:

$$V_w^e(r) = \begin{cases} \dfrac{-V_0 exp(-\delta r)}{\epsilon r} & \text{inside the core and the WL} \\ V_0 & \text{otherwise} \end{cases} \tag{3}$$

$$V_c(r) = \begin{cases} -\dfrac{e^2}{4\pi\epsilon r} & \text{inside the core and the WL} \\ 0 & \text{otherwise} \end{cases} \tag{4}$$

$\delta = 0.01$, $V_0 = |E_g(Si) - E_g(Si_{1-x}Ge_x)|$, and $r = \sqrt{x^2 + y^2 + (z-d)^2}$, where d is the position of impurity.

The expression for bandgap dependency on temperature with respect to material composition is given by [27]:

$$E_g^{SiGe}(T) = E_g^{Si}(0).(1-x) + E_g^{Ge}(0).x + C_g.(1-x)x - \frac{\alpha.T^2}{\beta + T} \tag{5}$$

where $E_g^{Si}(0) = 1.166$ eV, $E_g^{Ge}(0) = 0.7437$eV, $C_g = -0.4\,eV$, $\alpha = 4.73 \times 10^{-4}\,eV/K$ and $\beta = 636\,K$,.

The $Si_{1-x}Ge_x$ alloys are considered as Si-like material for $x < 0.85$. The formula for the effective mass's temperature-dependent change is [45]

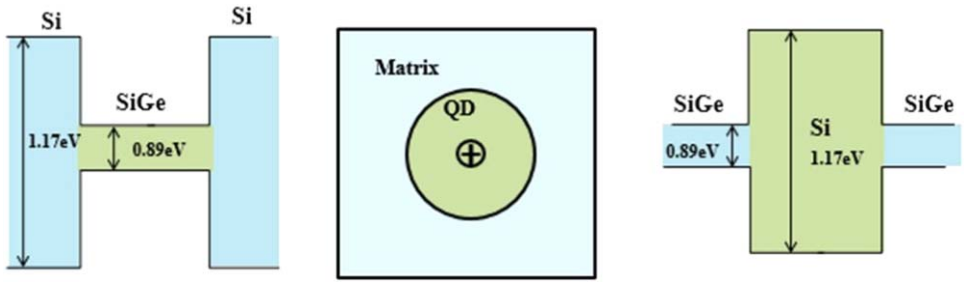



**Figure 1.** (a) Case-A: Bandgap diagram of *SiGe* QD in *Si* matrix (b)2D Cross section of QD (c) Case-B: *Si* QD in *SiGe* matrix.

$$m_e^*(T) = \frac{m_0}{1 + \frac{C_i}{E_g(T)}} \tag{6}$$

where $C_i = 3.19$ eV.

Position affects the system's dielectric constant as [46]

$$\epsilon\,(r_i) = \frac{\epsilon_{in}}{1 + \frac{r_i}{R}\left(\frac{\epsilon_{in}}{\epsilon_{out}} - 1\right)} \tag{7}$$

where R is the size of QD.

To analyze the optical properties, we use the well-known formalism based

Utilizing the well-known formalism [47–49], which is based on the density matrix method, we evaluate the optical properties in order to identify linear and non-linear (third-order) ACs and RICs. According to Boyd [50], whenever an electromagnetic field of a certain frequency interacts with a system, the polarisation changes and has both linear and non-linear components. As a result, we have optical rectification (OR), second harmonic generation (SHG), third harmonic generation (THG), and so on. Along with ACs and RICs, SHG and THG coefficients, which provide comprehensive information about the optical response of the system, are calculated with the use of second- and third-order susceptibilities. To see the details of the formulism please refer to our previous works [10, 27, 44, 51].

## 3. Results and discussion

We have calculated the energy spectra and optical properties of a donor impurity in Yukawa potential numerically by finite element method using COMSOL Multiphysics 5.5 software [52]. The parameters used in the numerical calculations for SiGe are as follows: $\sigma = 2.8 \times 10^{25}$ m$^{-3}$, the electron density, $n_r(\eta = 0.3) = 3.55$ represents the refractive index of the QD, $\varepsilon(\eta = 0.3) = 13.15$ is the static dielectric constant, $\Gamma_{if} = 1/0.38$ ps$^{-1}$ is the inverse of the relaxation time material [53, 54]. The exciton Bohr radius for this system is approx. 2.5nm, so we have taken the size of the QD radius comparable to this value (4.2 nm or 4.1 nm as the wavefunction is confined within the QD for these values). The effective mass of conductivity $m^*_{SiGe} = 0.26m_0$, where $m_0$ is the mass of free electrons. We have categorized the results into two parts (i) Temperature dependence for *SiGe* QD within *Si* Matrix (ii) Temperature dependence for *Si* QD within *SiGe* Matrix.

### 3.1. Temperature dependence for *SiGe* QD within *Si* Matrix

We have studied the energy spectra of the first six low-lying states for the *SiGe* QD within the *Si* matrix as this will give a better understanding of the optical response. Figure 2 shows the Variation of energy for the first six low-lying states with a different temperature for QD of radius 4.2 nm.

As we can see, the first and second excited states are degenerate, as well as the third and fourth excited states. Increasing the temperature increases the energy of the levels. This is due to an increase in the kinetic energy of the system. We have calculated the optical absorption coefficients(ACs) from the ground($E_1$) to the first excited state($E_2$) transition for different values of temperature.

Figure 3 shows the linear, non-linear, and total ACs and RICs for QD of radius 4.2 nm for a laser radiation intensity of $2^*10^{10}$ W m$^{-2}$. The result shows a blue shift with an increase in temperature. This outcome is expected as we have seen in figure 2 that the transition energy from the ground to the first excited state increases with an increase in temperature. The behavior of ACs and refractive index changes (RICs) is similar to the dependence of the two on dipole matrix elements and the transition energy is similar.

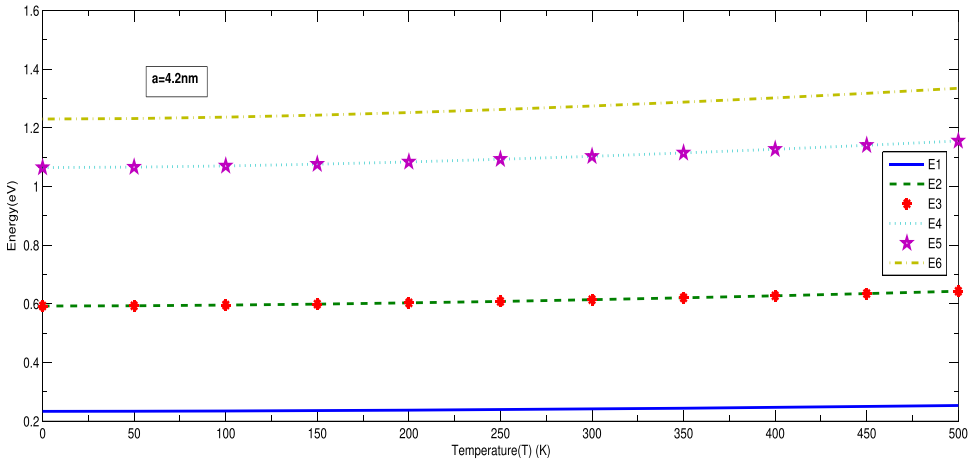



**Figure 2.** Variation of energy for first six low-lying states with a different temperature for QD of radius 4.2 nm.

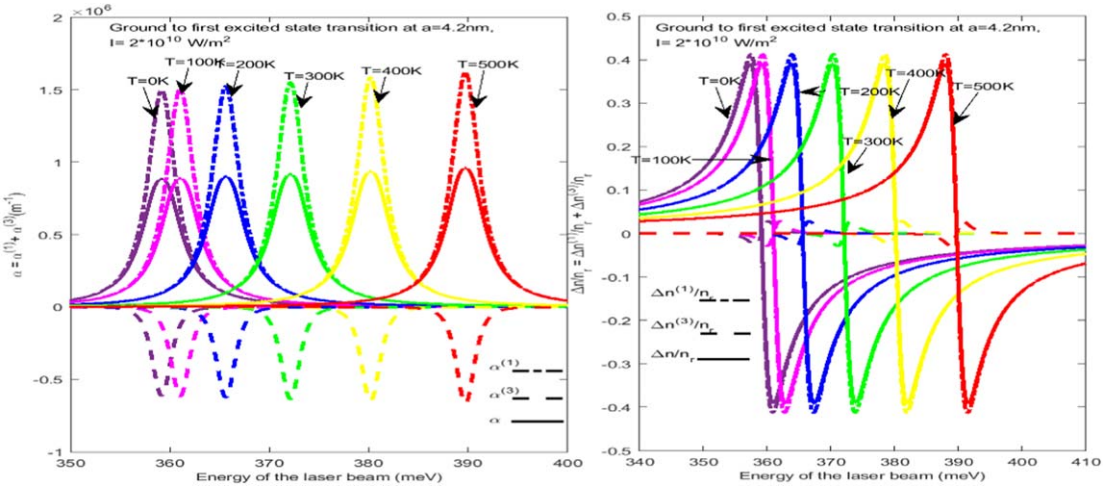



**Figure 3.** Linear, non-linear, and total absorption coefficients and RICs from ground to first excited state as a function of the photon energy for different temperatures for QD of radius 4.2 nm.

We observe a blue shift in peaks with rising temperatures. To understand the AC and RIC of different transitions with varying laser intensity we have plotted figure 4. This figure shows the linear, non-linear, and total ACs and RICs from ground to first excited state and second excited state to third excited state as a function of the photon energy for different intensities with temperature = 300 K for QD of radius 4.2 nm.

We observe that with an increase in the intensity of the laser beam, the bleaching effect comes into the picture. However, the value of intensity for which the bleaching effect appears for the ground to first excited state and second to third excited state transition is different which is expected. As the transition energy is different, so are the dipole matrix elements. The bleaching effect arises due to an increase in the non-linear component of AC with an increase in intensity. For the same set of intensities, the AC amplitude of the second to third excited state transition is higher than the ground to first excited state transition.

Another way of altering optical properties is by changing the size of the QD. This can be achieved by doing modifications in the fabrication conditions. Figure 5 shows the variation of six low-lying energy states with a change in the QD radius for a temperature of 300 K. Here we note that the energy of these states decreases with an increase in the size of the QD as that will enhance the volume which results in poor confinement. It is observed that the $E_2$ and $E_3$ states are degenerate and $E_4$ and $E_5$ states are degenerate.

The linear, non-linear, and total ACs for the ground to first excited state and second excited state to third excited state transitions as a function of the photon energy for different intensities with QD of radius 4.1 nm for a temperature of 300K are plotted. We observe that with an increase in the intensity, the total AC decreases as the non-linear AC increases which is opposite to the linear AC (which is constant as it is independent of the intensity).

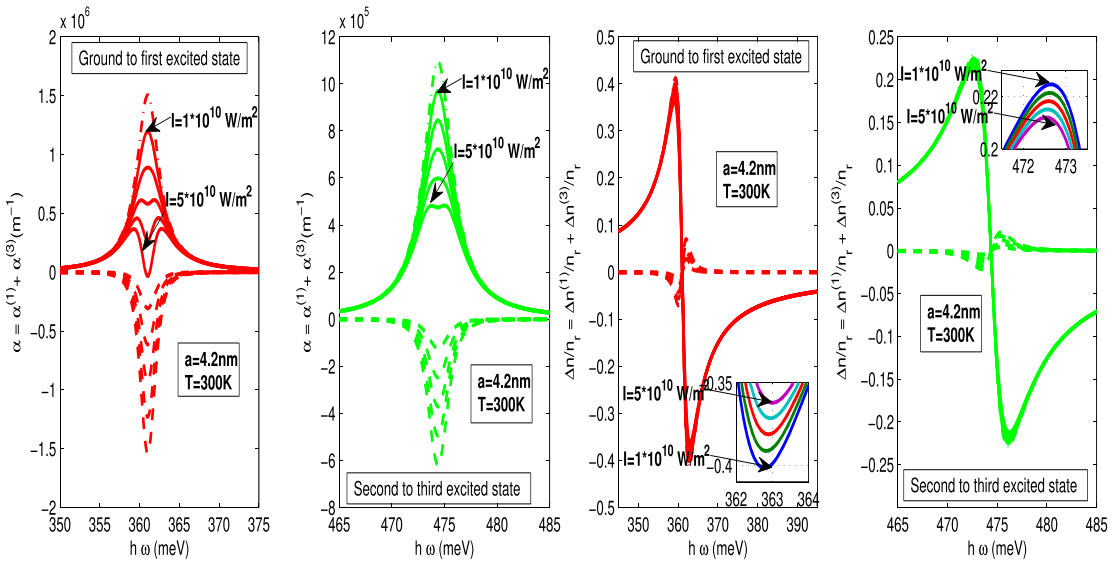



**Figure 4.** Linear, non-linear, and total absorption coefficients and refractive index changes from ground to first excited state and second excited state to third excited state as a function of the photon energy for different intensities with temperature = 300 K for QD of radius 4.2 nm.

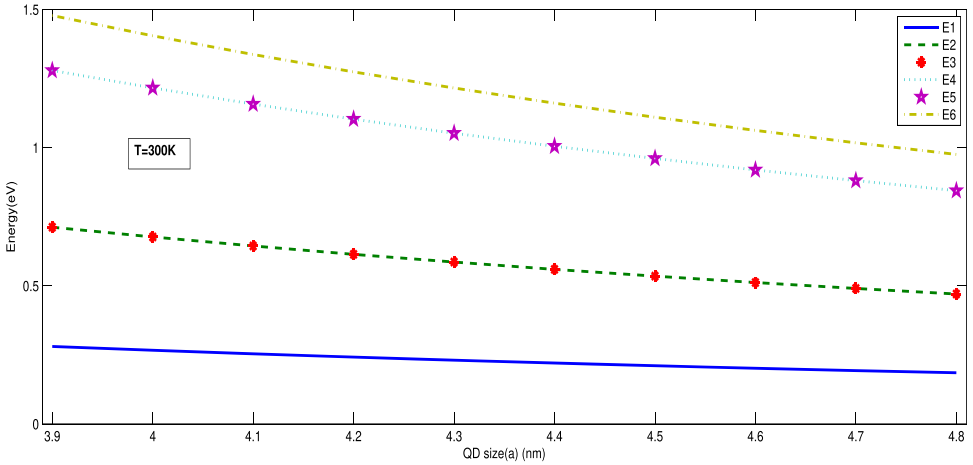



**Figure 5.** Variation of energy for first six low-lying states with different QD radius for a temperature of 300 K.

Another way of altering optical properties is by changing the size of the QD. This can be achieved by doing modifications to the fabrication conditions. Figure 5 shows the variation of six low-lying energy states with a change in the QD radius for a temperature of 300K. Here we note that the energy of these states decreases with an increase in the size of the QD as that will enhance the volume which results in poor confinement. It is observed that the $E_2$ and $E_3$ states are degenerate and the $E_4$ and $E_5$ states are degenerate.

To understand the role of intensity of the applied laser field and QD size, we have studied the optical response of the system in figure 6 and 7. Figure 6 shows that with an increase in the intensity of the laser field, the bleaching efffect arises in the absorption peaks. This is due to the increase in the nonlinear behaviour of the abdortion peaks and RIC curves. For study of QD size variation, we have plotted the linear, non-linear, and total AC in figure 7.

It has been observed that with an increase in QD size, redshift is observed. This is a consequence of increasing volume with an increase in size which leads to poor confinement.

### 3.2. Temperature dependence for *Si* QD within *SiGe* Matrix

The material we choose for the matrix and QD is very important as it controls the dynamics of the system. This will decide the potential barrier by which charge carriers are confined in the QD inside the matrix. Therefore to have a clear vision of this theory, we have calculated the results when within the *SiGe* matrix a *Si* QD is trapped which is shown in figure 1(c).

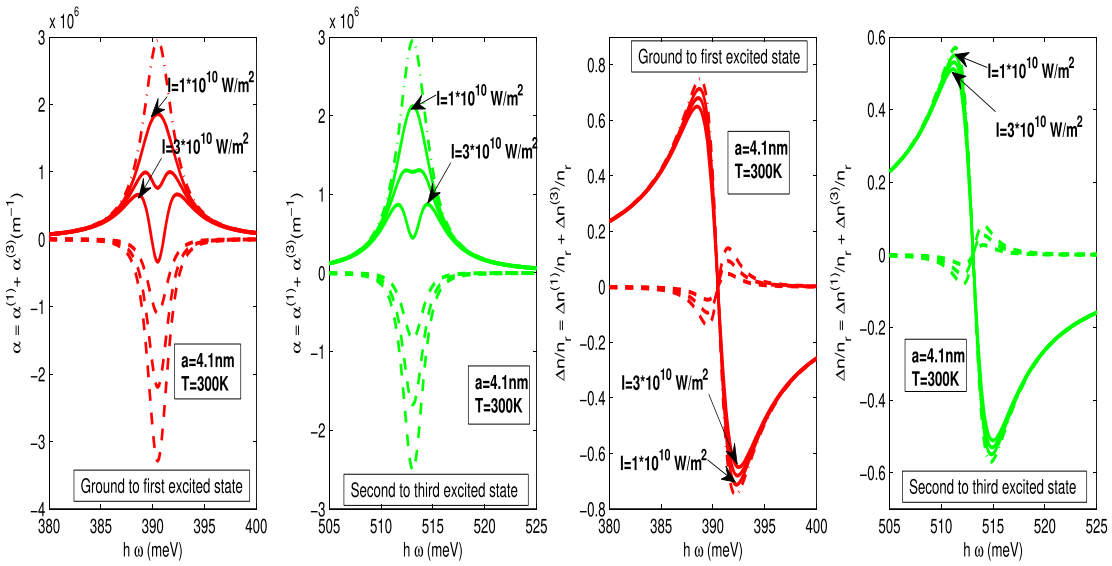



**Figure 6.** Linear, non-linear, and total absorption coefficients and refractive index changes from ground to first excited state and second excited state to third excited state as a function of the photon energy for different intensities with QD of radius 4.1 nm for a temperature of 300 K.

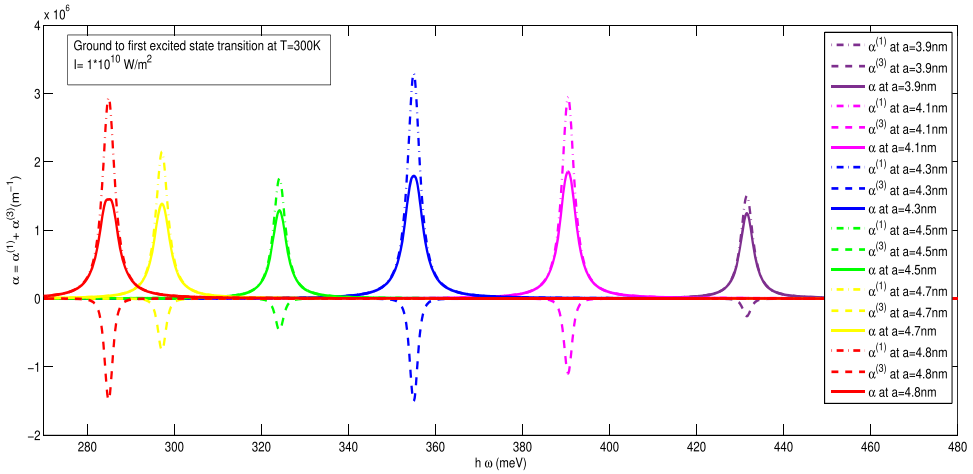



**Figure 7.** Linear, non-linear, and total absorption coefficients from ground to first excited state as a function of the photon energy for different QD of radius for a temperature of 300 K.

The variation of the energies of six low-lying states with temperature has been shown in figure 8. In this case too, the $E_2$, $E_3$ and $E_4$, $E_5$ states are degenerate. When comparing the two cases (case A and case B), we observe that the case B system has a lower energy of different states, which can be explained by the large energy bandgap of *Si* QD compared to *SiGe* QD.

For analyzing the optical response difference we have obtained AC change curves. Figure 9 shows ACs from ground to the first excited state as a function of the photon energy at different temperatures.

We observe a blue shift of optical resonance transition peaks for AC with an increase in temperature as visible in figure 9. This is due to the increase in the energy of the states with temperature (see figure 8).

Manipulation of these AC and RIC resonance peaks can be done by varying the intensity. Figure 10 shows linear, non-linear, and total ACs and RICs from ground to first excited state and second excited state to third excited state as a function of the photon energy for different intensities. We observe that with an increase in the intensity of the AC and RIC transition peaks the nonlinear component increases and hence the bleaching effect arises in the total AC and RIC peaks.

The variation of energy for the first six low-lying states with different QD radii at a temperature of 300 K is plotted in figure 11. $E_2$, $E_3$ and $E_4$, $E_5$ states are degenerate and on increasing the dot radius (i.e. increasing the volume and decreasing the strength) the energy of the different levels decreases.

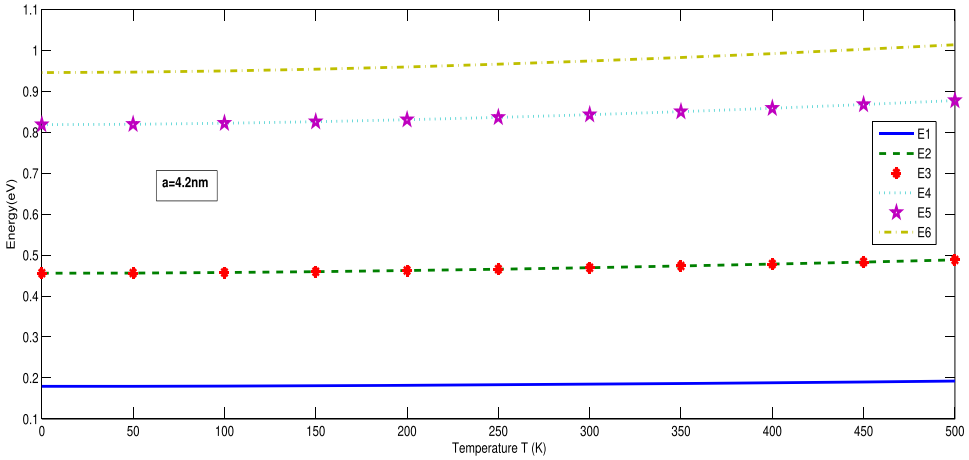



**Figure 8.** Variation of energy for first six low-lying states with a different temperature for QD of radius 4.2 nm.

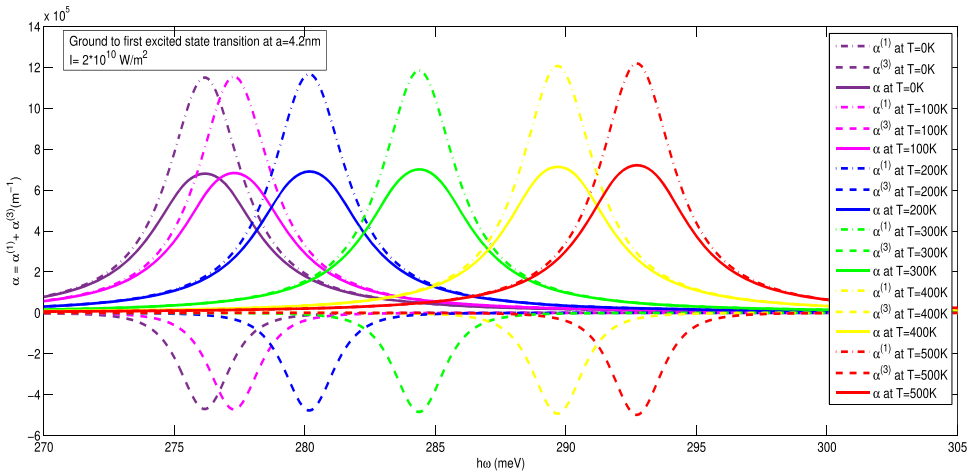



**Figure 9.** Linear, non-linear, and total absorption coefficients from ground to first excited state as a function of the photon energy for different temperatures for QD of radius 4.2 nm.

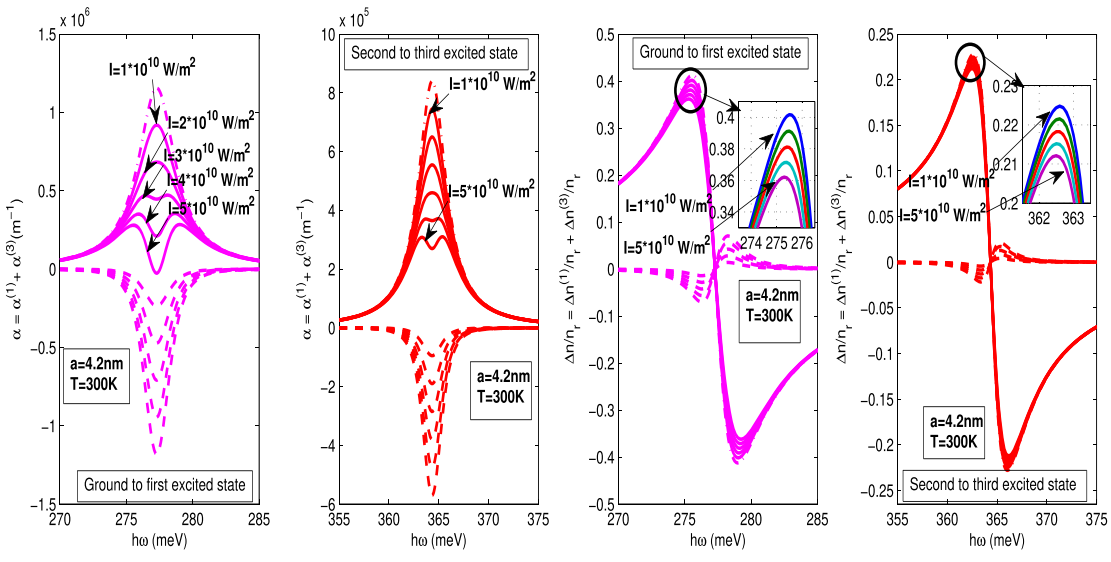



**Figure 10.** Linear, non-linear, and total absorption coefficients and refractive index changes from ground to first excited state and second excited state to third excited state as a function of the photon energy for different intensities with temperature = 300 K for QD of radius 4.2 nm.

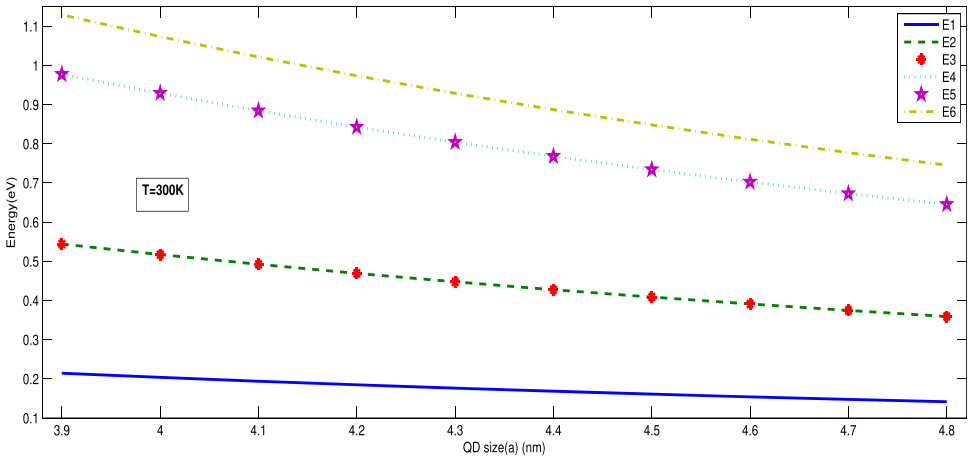



**Figure 11.** Variation of energy for first six low-lying states with different QD radius for the temperature of 300 K.

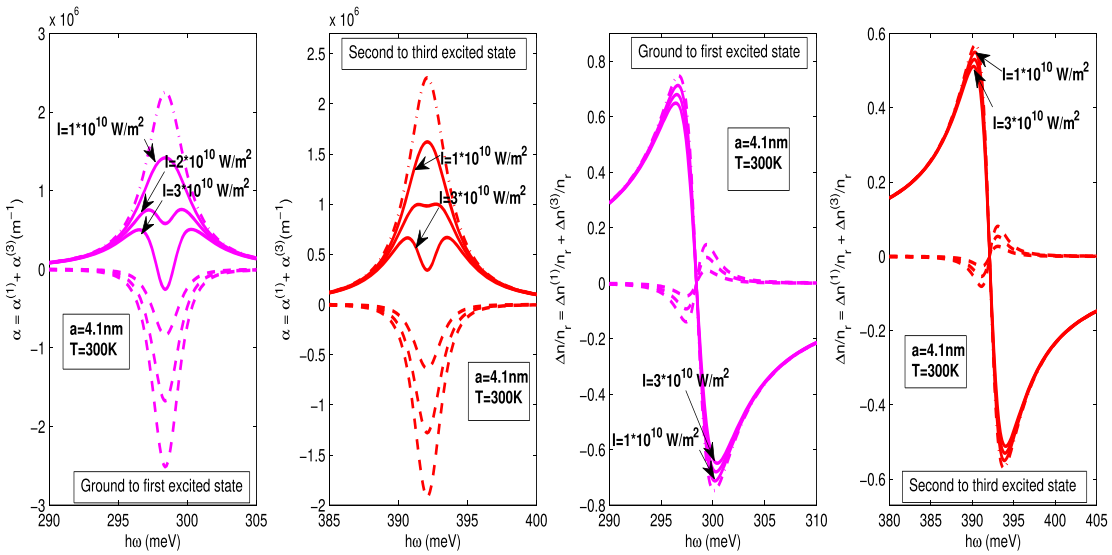



**Figure 12.** Linear, non-linear, and total absorption coefficients and refractive index changes from ground to first excited state and second excited state to third excited state as a function of the photon energy for different intensities with QD of radius 4.1 nm for a temperature of 300 K.

The effect of intensity on AC is shown in figure 12 and the impact of dot radius are shown in figure 13 respectively. We observe the bleaching effect with a rise in the intensity of the laser radiation.

Redshift is displayed by AC resonance peaks with an increase in the dot radius. The reason for blueshift is the decrease in the confinement strength with an increase in dot radius.

SHG and THG nonlinear optical response gives an insight into the response of the system. We have calculated these coefficients for different temperatures and QD sizes as a function of photon energy. Nonlinear microscopy is a major use of harmonic generation. One reason for exploiting nonlinear effects in microscopy, particularly harmonic production, is to improve transverse and longitudinal resolution. Because nonlinear processes are most efficiently activated in the region of greatest intensity of a focused laser beam, resolution is improved. Microscopy based on harmonic generation also has the advantage of separating the signal from undesirable background light caused by linear scattering of the input laser beam.

Figures 14(a) and (b) show SHG and THG for different dot sizes at T = 300 K for *SiGe*/*Si* QD as a function of photon energy respectively. With an increase in the dot size, we observe redshift as the increased volume will decrease the confinement effects. Figures 14(c) and (d) shows SHG and THG for the different temperatures at a = 4.2 nm for *SiGe*/*Si* QD as a function of the photon energy. We observe that with an increase in temperature,

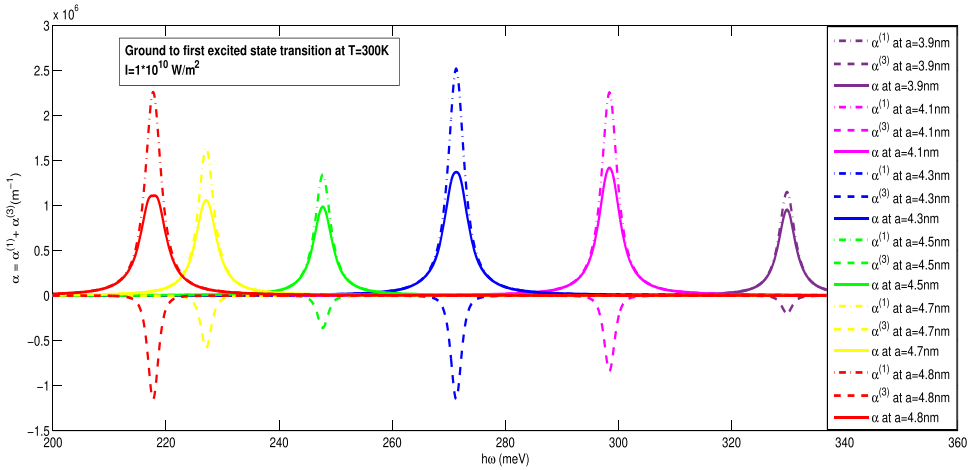



**Figure 13.** Linear, non-linear, and total absorption coefficients from ground to first excited state as a function of the photon energy for different QD of radius for a temperature of 300 K.

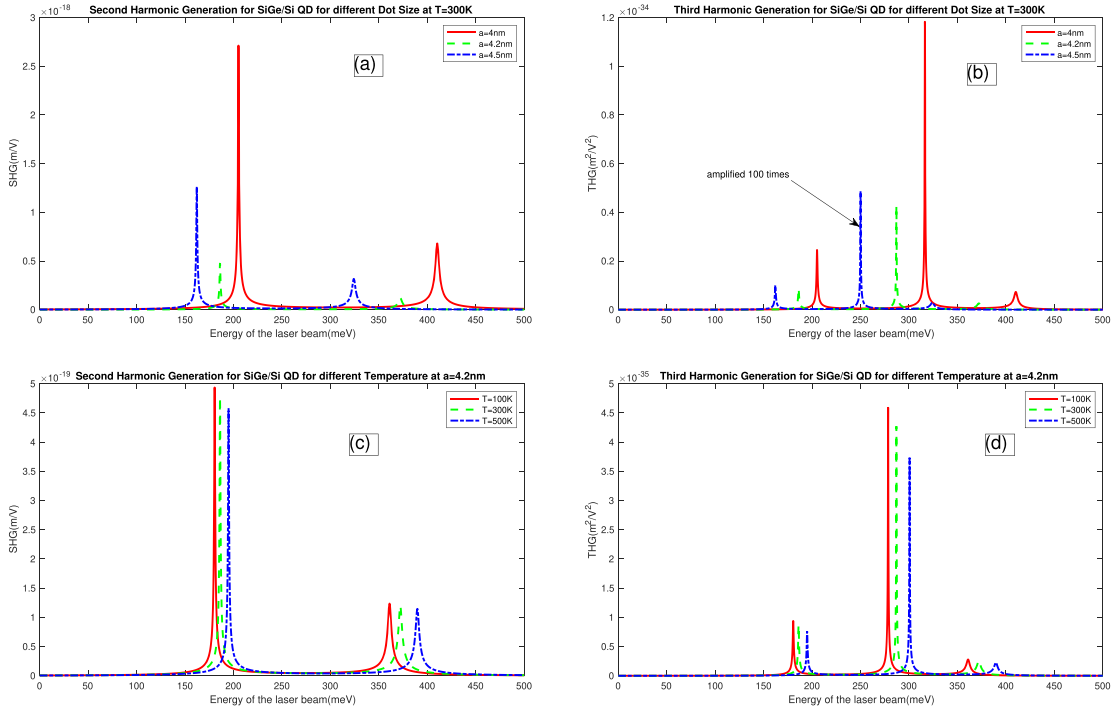



**Figure 14.** (a) Second harmonic generation for different dot size at T = 300 K for *SiGe*/*Si* QD as a function of the photon energy (b) Third harmonic generation for different dot size at T = 300 K for *SiGe*/*Si* QD as a function of the photon energy (c) Second harmonic generation for the different temperature at a = 4.2 nm for *SiGe*/*Si* QD as a function of the photon energy (d) Third harmonic generation for the different temperature at a = 4.2 nm for *SiGe*/*Si* QD as a function of the photon energy.

blueshift is observed in the harmonic peaks which are due to the increase in the kinetic energy which also increases the total energy.

Figures 15(a) and (b) show SHG and THG for different dot sizes at T = 300 K for *Si*/*SiGe* QD as a function of photon energy respectively. With an increase in the dot size, we observe redshift as the increased volume will decrease the confinement effects. Figures 15(c) and (d) shows SHG and THG for the different temperatures at a = 4.2 nm for *Si*/*SiGe* QD as a function of the photon energy. We observe that with an increase in temperature, blueshift is observed in the harmonic peaks which are due to the increase in the kinetic energy which also increases the total energy.

THG coefficients for CdS [55] QD are of the order of $10^{-15}$m$^2$V$^{-2}$ and for the *SiGe* [27] oblate and prolate QD in perpendicular external electric field case are of the order of $10^{-22}$m$^2$V$^{-2}$ and for SHG, the order of amplitude is $10^{-12}$m V$^{-1}$ for the *SiGe* oblate and prolate QD in perpendicular external electric field case and for

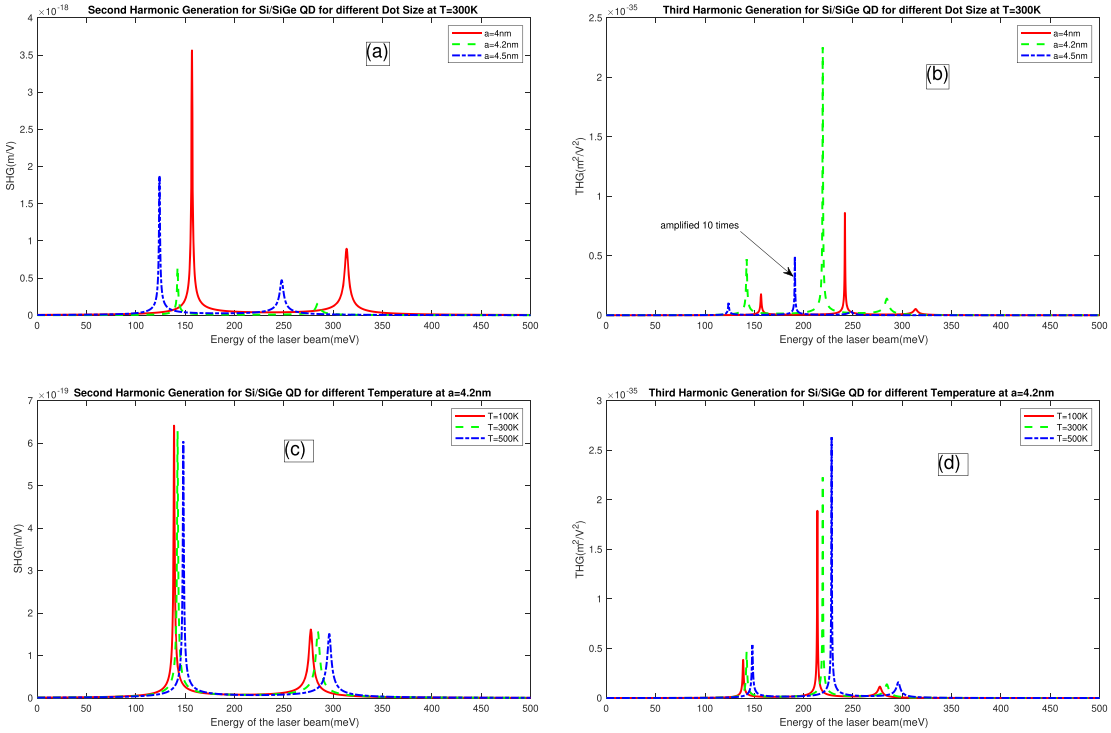



**Figure 15.** (a) Second harmonic generation for different dot size at T = 300 K for *Si*/*SiGe* QD as a function of the photon energy (b) Third harmonic generation for different dot size at T = 300 K for *Si*/*SiGe* QD as a function of the photon energy (c) Second harmonic generation for the different temperature at a = 4.2 nm for *Si*/*SiGe* QD as a function of the photon energy (d) Third harmonic generation for the different temperature at a = 4.2 nm for *Si*/*SiGe* QD as a function of the photon energy.

CdS QD it is of the order of $10^{-9}$m $V^{-1}$. So, in Yukawa potential confinement, we observe that the magnitude of the *SiGe* spherical QD for SHG decreases by approx. $10^5$ times and for THG it is very small of the order of $10^{-35}$m$^2$ $V^{-2}$.

## 4. Conclusion

We have investigated the energy spectra and optical properties of a donor impurity in Yukawa potential for *SiGe* QD within *Si* Matrix and vice-versa. We have observed a bleaching effect with an increase in the intensity of the laser radiation. Blueshift is displayed by nonlinear optical properties i.e. AC, RIC, SHG, and THG with an increase in the temperature, and redshift is observed with an increase in the dot radius. The understanding of these manipulating factors has applications in the manufacturing of optoelectronic devices.

## Acknowledgments

LMP acknowledges financial support from ANID through Convocatoria Nacional Subvención a Instalación en la Academia Convocatoria Año 2021, Grant SA77210040. DL acknowledges partial financial support from the Centers of Excellence with BASAL/ANID financing, AFB220001, CEDENNA.

## Data availability statement

All data that support the findings of this study are included within the article (and any supplementary files).

## ORCID iDs

Varsha https://orcid.org/0000-0002-6607-1966
D Laroze https://orcid.org/0000-0002-6487-8096
L M Pérez https://orcid.org/0000-0002-2915-309X
V Prasad https://orcid.org/0000-0002-0154-3221
E Feddi https://orcid.org/0000-0001-6641-3623

## References


[1] Ekimov A I and Onushchenko A A 1982 Quantum size effect in the optical-spectra of semiconductor micro-crystals *Soviet Physics Semiconductors-USSR* **16** 775–8
[2] Drbohlavova J, Adam V, Kizek R and Hubalek J 2009 Quantum dots-characterization, preparation and usage in biological systems *Int. J. Mol. Sci.* **10** 656–73
[3] Cochrane L *et al* 2022 Parametric amplifiers based on quantum dots *Phys. Rev. Lett.* **128** 197701
[4] Wang X, Sun G, Li N and Chen P 2016 Quantum dots derived from two-dimensional materials and their applications for catalysis and energy *Chem. Soc. Rev.* **45** 2239–62
[5] Manikandan A, Chen Y Z, Shen C C, Sher C W, Kuo H C and Chueh Y L 2019 A critical review on two-dimensional quantum dots (2D QDs): from synthesis toward applications in energy and optoelectronics *Prog. Quantum Electron.* **68** 100226
[6] GarcÁa de Arquer F P, Talapin D V, Klimov V I, Arakawa Y, Bayer M and Sargent E H 2021 Semiconductor quantum dots: technological progress and future challenges *Science* **373** eaaz8541
[7] Yoffe A D 2001 Semiconductor quantum dots and related systems: electronic, optical, luminescence and related properties of low dimensional systems *Adv. Phys.* **50** 1–208
[8] Chembo Y K, Brunner D, Jacquot M and Larger L 2019 Optoelectronic oscillators with time-delayed feedback *Rev. Mod. Phys.* **91** 035006
[9] Abolfath R M, Hawrylak P and Žutić I 2007 Tailoring magnetism in quantum dots *Phys. Rev. Lett.* **98** 207203
[10] Kria M, Varsha, Farkous M, Prasad V, Dujardin F, PÃrez L M, Laroze D and Feddi E 2021 Wetting layer and size effects on the nonlinear optical properties of semi oblate and prolate $Si_{0.7}Ge_{0.3}$/Si quantum dots *Curr. Appl. Phys.* **25** 1–11
[11] Lu L, Xie W and Shu Z 2011 Combined effects of hydrostatic pressure and temperature on nonlinear properties of an exciton in a spherical quantum dot under the applied electric field *Phys. B.* **406** 3735–40
[12] Karabulut I and Baskoutas S 2008 Linear and nonlinear optical absorption coefficients and refractive index changes in spherical quantum dots: effects of impurities, electric field, size, and optical intensity *J. Appl. Phys.* **103** 073512
[13] Safarpour G, Zamani A, Izadi M A and Ganjipour H 2014 Laser radiation effect on the optical properties of a spherical quantum dot confined in a cylindrical nanowire *J. Lumin.* **147** 295–303
[14] Farkoush B A, Safarpour G and Zamani A 2013 Linear and nonlinear optical absorption coefficients and refractive index changes of a spherical quantum dot placed at the center of a cylindrical nano-wire: Effects of hydrostatic pressure and temperature *Superlattices Microstruct.* **59** 66–76
[15] Varsha, Silotia P and Prasad V 2020 Study of optical properties of Wannier-Mott exciton in spherical quantum dot in Kratzer potential *AIP Conference Proceedings, AIP Publishing* 2220020154
[16] Jahan K L, Boda A and Chatterjee A 2015 Ground state energy of an exciton in a spherical quantum dot in the presence of an external magnetic field *AIP Conference Proceedings, AIP Publishing* 1661 080008
[17] Flórez J and Camacho Á 2011 Excitonic effects on the second-order nonlinear optical properties of semi-spherical quantum dots *Nanoscale Res. Lett.* **6** 1–6
[18] Prasad V and Silotia P 2011 Effect of laser radiation on optical properties of disk shaped quantum dot in magnetic fields *Phys. Lett.* A **375** 3910–5
[19] Shi L and Yan Z W 2019 Optical properties of an exciton trapped by an ionized donor in ellipsoidal quantum dots under electric field and hydrostatic pressure *Int. J. Mod. Phys.* B **33** 1950108
[20] Shahzadeh M and Sabaeian M 2014 Erratum: The effects of wetting layer on electronic and optical properties of intersubband P-to-S transitions in strained dome-shaped *InAs/GaAs* quantum dots *AIP Adv.* **4** 099901
[21] Vorobiev Y V, Torchynska T V and Horley P P 2013 Effect of aspect ratio on energy of optical transitions in a pyramid-shaped quantum dot *Physica E* **51** 42–7
[22] Hwang T M, Lin W W, Wang W C and Wang W 2004 Numerical simulation of three dimensional pyramid quantum dot *J. Comput. Phys.* **196** 208–32
[23] Oukerroum A, Feddi E, Bailach J B, Martínez-Pastor J, Dujardin F and Assaid E 2010 On the anomalous Stark effect in a thin disc-shaped quantum dot *J. Phys. Condens. Matter* **22** 375301
[24] You J and Guo K 2022 Electronic and optical properties of cubic quantum dots subjected to terahertz laser field *Photonics and Nanostructures-Fundamentals and Applications* **49** 100994
[25] Hong H *et al* 2021 Giant enhancement of optical nonlinearity in two-dimensional materials by multiphoton-excitation resonance energy transfer from quantum dots *Nat. Photonics* **15** 510–5
[26] Mittelstädt A, Schliwa A and Klenovský P 2022 Modeling electronic and optical properties of III-V quantum dots-Selected recent developments *Light: Science & Applications* **11** 1–14
[27] Kria M, Hamdaoui J E, PÁ©rez L M, Prasad V, El-Yadri M, Laroze D and Feddi E M 2021 Quantum confined stark effect on the linear and nonlinear optical properties of SiGe/Si semi oblate and prolate quantum dots grown in Si wetting layer *Nanomaterials* **11** 1513
[28] Perlin P, Kisielowski C, Iota V, Weinstein B A, Mattos L, Shapiro N A, Kruger J, Weber E R and Yang J 1998 InGaN/GaN quantum wells studied by high pressure, variable temperature, and excitation power spectroscopy *Appl. Phys. Lett.* **73** 2778–80
[29] Dawson P, Rubel O, Baranovskii S D, Pierz K, Thomas P and Göbel E O 2005 Temperature-dependent optical properties of In As/Ga As quantum dots: Independent carrier versus exciton relaxation *Phys. Rev.* B **72** 235301
[30] Liang S and Xie W 2011 Effects of the hydrostatic pressure and temperature on optical properties of a hydrogenic impurity in the disc-shaped quantum dot *Physica B* **406** 2224–30
[31] Kirak M, Altinok Y and Yilmaz S 2013 The effects of the hydrostatic pressure and temperature on binding energy and optical properties of a donor impurity in a spherical quantum dot under external electric field *J. Lumin.* **136** 415–21
[32] Edwards J P, Gerber U, Schubert C, Trejo M A and Weber A 2017 *Prog. Theor. Exp. Phys.* **2017** 083A01 1
[33] Lumb S, Lumb S and Prasad V 2015 Photoexcitation and ionization of a hydrogen atom confined by a combined effect of a spherical box and Debye plasma *Phys. Lett.* A **379** 1263–9
[34] Bale H P, Máarif M, Suparmi A and Cari C 2019 Bound state energy of spherical quantum dot with Yukawa potential influenced by static electric and magnetic fields *AIP Conference Proceedings, AIP Publishing* 2202 020007
[35] MÁ©ndez-Camacho R, Cruz-Hernández E and Castaneda-Priego R 2017 Wigner crystallization in quantum wires within the Yukawa approximation *Phys. Rev.* B **95** 085437
[36] Nomura W, Yatsui T, Kawazoe T, Naruse M and Ohtsu M 2010 Structural dependency of optical excitation transfer via optical near-field interactions between semiconductor quantum dots *Appl. Phys.* B **100** 181–7
[37] Ohtsu M, Kobayashi K, Kawazoe T, Sangu S and Yatsui T 2002 Nanophotonics: design, fabrication, and operation of nanometric devices using optical near fields *IEEE J. Sel. Top. Quantum Electron.* **8** 839–62

[38] Edet C O, Ikot A N, Okorie U S, Rampho G J, Ramantswana M, Horchani R, Abdullah H, Vinasco J A, Duque C A and Abdel-Aty A H 2021 Persistent current, magnetic susceptibility, and thermal properties for a class of Yukawa potential in the presence of external magnetic and Aharanov-Bohm fields *Int. J. Thermophys.* **42** 1–18
[39] Napsuciale M and Rodríguez S 2021 Complete analytical solution to the quantum Yukawa potential *Phys. Lett.* B **816** 136218
[40] Horchani R, Al-Aamri H, Al-Kindi N, Ikot A N, Okorie U S, Rampho G J and Jelassi H 2021 Energy spectra and magnetic properties of diatomic molecules in the presence of magnetic and AB fields with the inversely quadratic Yukawa potential *Eur. Phys. J.* D **75** 1–13
[41] Ji X H, He Y Y, Jiao L G, Liu A and Ho Y K 2021 Probability density of the Yukawa particle at the origin: Numerical calculation and analytical solution *Phys. Lett.* B **823** 136718
[42] Jiao L G, Xie H H, Liu A, Montgomery H E and Ho Y K 2021 Critical screening parameters and critical behaviors of one-electron systems with screened Coulomb potentials *J. Phys. B: At. Mol. Opt. Phys.* **54** 175002
[43] Haddara Y M, Ashburn P and Bagnall D M 2017 Silicon-germanium properties, growth and applications *Springer Handbook of Electronic and Photonic Materials, Springer Handbooks* ed S Kasap and P Capper (Cham: Springer)
[44] Varsha, Lakaal K, Kria M, Hamdaoui J E, Prasad V, Feddi E, Laroze D, PÁ©rez L M and Ramos M E 2022 Lattice deformation and potential effects on linear and nonlinear optical properties of doped SiGe quantum dot encapsulated in Si matrix *Eur. Phys. J Plus* **137** 1–13
[45] Yu P Y and Cardona M 1988 *Fundamentals of Semiconductors* (Berlin: Springer)
[46] Aghoutane N, Feddi E, El-Yadri M, Bailach J B, Dujardin F and Duque C A 2017 Magnetic field and dielectric environment effects on an exciton trapped by an ionized donor in a spherical quantum dot *Superlattices Microstruct.* **111** 1082–92
[47] Vahdani M R K and Rezaei G 2009 Linear and nonlinear optical properties of a hydrogenic donor in lens-shaped quantum dots *Phys. Lett.* A **373** 3079–84
[48] Kria M, El-Yadri M, Aghoutane N, Paŕez L M, Laroze D and Feddi E 2020 Forecasting and analysis of nonlinear optical responses by tuning the thickness of a doped hollow cylindrical quantum dot *Chin. J. Phys.* **66** 444–52
[49] Vahdani M R K and Rezaei G 2010 Intersubband optical absorption coefficients and refractive index changes in a parabolic cylinder quantum dot *Phys. Lett.* A **374** 637–43
[50] Boyd R W 2003 *Nonlinear Optics* 2nd edn (New York: Academic)
[51] Kria M, Nautiyal V V, Lakaal K, El Hamdaoui J, PÁ©rez L M, Varsha, Laroze D, Prasad V, Long G and Feddi E 2022 Rashba effect on linear and nonlinear optical properties of a cylindrical core/shell heterojunction quantum dot *Frontiers in Physics* 669
[52] COMSOL Multiphysics software version 5.5 (www.comsol.com) 14 Nov 2019
[53] Levinshtein M E, Rumyantsev S L and Shur M S 2001 *Properties of Advanced Semiconductor Materials GaN, AIN, InN, BN, SiC,SiGe* (Hoboken, NJ, USA: Wiley)
[54] Sasso G, Rinaldi N, Matz G and Jungemann C 2009 Accurate mobility and energy relaxation time models for SiGe HBTs numerical simulation *Proceedings of the International Conference on Simulation of Semiconductor Processes and Devices (San Diego, CA, USA)*
[55] Karabulut I and Baskoutas S 2009 Second and third harmonic generation susceptibilities of spherical quantum dots: effects of impurities, electric field and size *Journal of Computational and Theoretical Nanoscience* **6** 153–6